Molecules and Cells

Comparative Interactomes of VRK1 and VRK3 with Their Distinct Roles in the Cell Cycle of Liver Cancer

Namgyu Lee[1,5], Dae-Kyum Kim[3,4,6], Seung Hyun Han[1,6], Hye Guk Ryu[1], Sung Jin Park[1], Kyong-Tai Kim[1,2,*], and Kwan Yong Choi[1,2,*]

[1]Department of Life Science, [2]Department of Integrative Biosciences and Biotechnology, Pohang University of Science and Technology, Pohang 37673, Korea, [3]Donnelly Centre, Departments of Molecular Genetics and Computer Science, University of Toronto, Toronto, Canada, [4]Lunenfeld-Tanenbaum Research Institute, Mount Sinai Hospital, Toronto, Canada, [5]Present address: Department of Molecular, Cell and Cancer Biology, University of Massachusetts Medical School, Worcester, Massachusetts, USA, [6]These authors contributed equally to this work.
*Correspondence: kchoi@postech.ac.kr (KYC); ktk@postech.ac.kr (KTK)
http://dx.doi.org/10.14348/molcells.2017.0108
www.molcells.org

Vaccinia-related kinase 1 (VRK1) and VRK3 are members of the VRK family of serine/threonine kinases and are principally localized in the nucleus. Despite the crucial roles of VRK1/VRK3 in physiology and disease, the molecular and functional interactions of VRK1/VRK3 are poorly understood. Here, we identified over 200 unreported VRK1/VRK3-interacting candidate proteins by affinity purification and LC-MS/MS. The networks of VRK1 and VRK3 interactomes were found to be associated with important biological processes such as the cell cycle, DNA repair, chromatin assembly, and RNA processing. Interactions of interacting proteins with VRK1/VRK3 were confirmed by biochemical assays. We also found that phosphorylations of XRCC5 were regulated by both VRK1/VRK3, and that of CCNB1 was regulated by VRK3. In liver cancer cells and tissues, VRK1/VRK3 were highly upregulated and its depletion affected cell cycle progression in the different phases. VRK3 seemed to affect S phase progression and G2 or M phase entry and exit, whereas VRK1 affects G1/S transition in the liver cancer, which could be explained by different interacting candidate proteins. Thus, this study not only provides a resource for investigating the unidentified functions of VRK1/VRK3, but also an insight into the regulatory roles of VRK1/VRK3 in biological processes.

Keywords: ESI-MS/MS, interactome, VRK1, VRK3

INTRODUCTION

Vaccinia-related kinases (VRKs) are a family of serine/threonine kinases, composed of VRK1-3 in mammals (Klerkx et al., 2009). They share a similar serine/threonine protein kinase domain (Klerkx et al., 2009). VRK1 and VRK3 have a nuclear localization signal on the C- and N-terminals, respectively, whereas VRK2 contains a transmembrane domain on the C-terminal (Lopez-Borges and Lazo, 2000). Among three VRK family proteins, VRK1 is the most extensively studied protein. Some of proteins that interact with VRK1 are characterized (Valbuena et al., 2011), and reports suggest that VRK1 plays a crucial role in cancer progression by targeting several substrates involved in the cell cycle or DNA repair (Lee et al., 2015b; Monsalve et al., 2016; Valbuena et al., 2011). p53 has been identified as a substrate protein regulated by VRK1 (Lopez-Borges and Lazo, 2000). VRK1 specifically phosphorylates p53 at Thr18, leading to the stabilization and subsequent accumulation of p53 (Lopez-Borges and Lazo, 2000; Lopez-Sanchez et al., 2014; Vega et al., 2004). VRK1

Received 4 July, 2017; accepted 10 July, 2017; published online 20 September, 2017

eISSN: 0219-1032

phosphorylates barrier-to-autointegration factor (BAF), which induces the disassembly of a complex containing chromatin, LEM proteins, and BAF (Gorjanacz et al., 2007; Nichols et al., 2006). Furthermore, VRK1 binds and phosphorylates several transcription factors such as ATF2 (Sevilla et al., 2004b), CREB1 (Kang et al., 2008), and c-Jun (Sevilla et al., 2004a) and histone proteins such as mitotic histone H3 (Kang et al., 2007), macroH2A1 (Kim et al., 2012), and H2AX (Salzano et al., 2015). In addition, HnRNP A1 is phosphorylated by VRK1 to stimulate telomerase (Choi et al., 2012). NBS1 also interacts with and is phosphorylated by VRK1 at Ser343, which stabilizes NBS1 protein in response to DNA damage (Monsalve et al., 2016).

Compared with VRK1, VRK3-interacting proteins have been less identified. VRK3 interacts with the phosphatase VHR and inhibits its phosphatase activity in a kinase-independent manner (Kang and Kim, 2006). Indeed, VRK3 was initially reported to be a pseudokinase (Nichols and Traktman, 2004). However, we confirmed the kinase activity of VRK3 by demonstrating the VRK3-mediated phosphorylation of BAF at Ser 4 (Park et al., 2015). CDK5/p35 complex was identified as a regulator of VRK3 by phosphorylating VRK3 at Ser 108, which resulted in increase of its affinity to VHR (Song et al., 2016a). VRK3 also interacts with HSP70 and promotes nuclear localization of glutamate-induced HSP70, which leads to activation of VHR activity (Song et al., 2016b). Due to the limited numbers of identified binding partners of VRKs, their roles in various biological processes remain elusive. Thus, it is important to identify novel interacting proteins of VRKs to clarify their roles.

Though only limited numbers of proteins were identified as interacting proteins of VRK1 or VRK3, their crucial roles during cell division seem to be obvious. VRK1 depletion induces the G1 arrest by downregulating cyclin D1 and p-Rb, and upregulating p21 and p27 in hepatocellular carcinoma (HCC), suggesting the crucial role of VRK1 in G1/S transition (Lee et al., 2015b). Regulation of cyclin D1 expression by VRK1 is mediated by phosphorylating the CREB transcription factor which upregulated the mRNA level of cyclin D1 (Kang et al., 2008; Lee et al., 2015b). VRK1 also coordinates several steps of mitosis. Phosphorylated VRK1 by polo-like kinase promotes Golgi fragmentation in G2/M phase (Lopez-Sanchez et al., 2009). Chromatin condensation, one of the crucial steps in mitosis, is enhanced via phosphorylation of histone H3 on Ser 10 by VRK1 (Lopez-Sanchez et al., 2009). Interestingly, nuclear envelope assembly and disassembly during mitosis are regulated by both VRK1 and VRK3 through the phosphorylation of BAF. During mitosis, VRK1 phosphorylates BAF in Ser 4, Thr 2 and Thr 3, which results in nuclear envelope disassembly required for the progression of mitosis (Gorjanacz et al., 2007; Nichols et al., 2006). During interphase, phosphorylation of BAF on Ser 4 by VRK3 promoted the disassembly of BAF, LEM proteins, and chromatin, which might result in the DNA replication (Park et al., 2015). Interaction of BAF with both VRK1 and VRK3 may imply the functional links during the specific biological processes. At the same time, distinct phosphorylation sites of BAF by VRK1 or VRK3, and involvement of phosphorylated BAF by VRK1 or VRK3 in the different steps during the cell cycle might suggest their distinct roles during the cell cycle. Comparing the interactomes of the same family proteins could provide new insights into their functional differences and redundancies. For instance, the phylogenetic relationships and functional similarities among 11 histone deacetylases (HDACs) were observed by building a global protein interaction network for HDACs (Joshi et al., 2013). We previously compared the interactomes of two sirtuin family proteins, SIRT6 and SIRT7, and revealed their functional links to aging based on shared interacting proteins (Lee et al., 2014). Thus, comparing the interactomes of VRK1 and VRK3 should help to systematically identify global interaction networks and differences in interacting proteins and to reveal their common or distinct roles in specific biological processes such as cell cycle.

In this study, we identified and compared VRK1- and VRK3-interacting candidate proteins by affinity purification and mass spectrometry under the same experimental conditions. We identified 153 interacting candidate proteins for VRK1 and 92 interacting candidate proteins for VRK3, including BAF, in agreement with previous findings. VRK1 and VRK3 shared 40 common interacting candidate proteins, indicating functional links between VRK1 and VRK3. The functional networks of the VRK1 and VRK3 interactomes were closely associated with the cell cycle, DNA repair, chromatin assembly, and RNA processing. The associations of nine interacting proteins with VRK1/VRK3 were further confirmed by co-immunoprecipitation and immunofluorescent staining. Phosphorylation levels of XRCC5 in serine residues were upregulated by VRK1/VRK3 overexpression. The phosphorylation of CCNB on threonine residues was specifically regulated by VRK3. We also found that VRK1 and VRK3 have distinct roles on cell cycle progression in liver cancer. VRK3 silencing induced S phase and G2/M phase arrest, whereas VRK1 silencing induced G1 arrest in the liver cancer, which could be explained by their distinct interatomic proteins involved in cell cycle progression. Our approaches and findings should be a valuable resource for investigating VRK1/VRK3 functions in the cell cycle, DNA repair, RNA processing, and chromatin assembly.

MATERIALS AND METHODS

Co-immunoprecipitation

Cells were harvested 24 h after transfection in cold PBS and centrifuged at 800 *g*. Cells were lysed with a lysis buffer containing 50 mM Tris-HCl, pH 7.4, 150 mM NaCl, 5 mM EDTA, 0.2% Triton X-100 and the inhibitor cocktail of proteases and phosphateases (Complete ULTRA Tablet and PhosSTOP, Roche). VRK1/VRK3 or p53, and their interacting proteins were pulled down with anti-flag M2 affinity gel (Sigma), eluted by boiling with Laemmli 2× Sample Buffer (Sigma) at 100℃ for 5 min, and then subjected to Coomassie blue staining, Western blotting or in-solution digestion.

In-solution digestion

Proteins were digested with trypsin, as described in a previous study, with some modifications (Choi et al., 2011). Briefly, eluted proteins were lyophilized and resolved in a diges-

tion solution of 6 M urea and 40 mM ammonium bicarbonate in high-performance liquid chromatography (HPLC)-grade water. Protein reduction was performed with 5 mM Tris (2-arboxyethyl) phosphine hydrochloride for 1 h, followed by alkylation with 25 mM iodoacetamide in the dark for 30 min at room temperature. The sample was in-solution digested with 5 ng/mL sequencing-grade modified trypsin (Promega) for 16 h at 37℃.

Nano-LC-MS/MS

Peptides were analyzed using mass spectrometry, as described previously, with some modifications (Choi et al., 2011). Tryptic peptides from in-gel digestion were separated using a homemade microcapillary column (75 μm x 12 cm) packed with C18 resin (Michrom Bioresources). Samples were eluted using a linear gradient of a mixture of solvents A (0.1% formic acid in 2% Acetonitrile) and B (0.1% formic acid in 98% Acetonitrile), where the percentage of the latter mobile phase increased over 120 min at a flow rate of 0.26 μl/min: 2-50% over 94 min, 50-90% over 6 min, 90% over 6 min, 90-2% over 6 min, and 2% over 8 min. Eluted peptides were analyzed with an LTQ Velos Orbitrap mass spectrometer (Thermo Finnigan) equipped with nano-ESI. MS precursor ion scans were acquired within a m/z range between 150 and 2000. The five most abundant ions detected in the precursor MS scan were dynamically selected for MS/MS analyses. Collision-induced dissociations of the selected precursor ions were performed in an ion trap (LTQ) with 35% normalized collision energy. We employed dynamic exclusion to increase the size of proteome to be detected as follows: repeat count for dynamic exclusion = 1, repeat duration = 30 s, dynamic exclusion duration = 180 s, and list size of dynamic exclusion = 50.

Identification and quantification of proteins

Peak lists of MS data were generated, and identification/quantification of peptides and proteins from three technical replicates of LC-MS/MS data were performed using the MaxQuant quantification tool with Andromeda search engine (version 1.3.0.5). The top 10 peaks per 100 Da were used for analysis. Enzyme specificity for trypsin was used. The minimal peptide length was six amino acids, and two mis-cleavages were allowed. Variable modification options were employed for oxidation of methionine (15.995 Da) and carbamidomethylation of cysteine (57.021 Da). Tolerance was set to 10 ppm for precursor ions and 0.8 Da for fragment ions. Swiss-Prot database (Homo sapiens reference proteome set, release 2013_01, 20,226 entries) with added contaminants and reverse sequences was used. For peptide and protein identification, 1% false discovery rate was determined by accumulating 1% of reverse database hits. Common peptides shared by two proteins were combined and reported as one protein group. The first majority protein ID was selected as the representative protein of each group, and used as protein ID for further analysis. For comparison of samples, we used label-free quantification with a minimum of two ratio counts to determine the normalized protein label-free quantification (LFQ) intensity (Luber et al., 2010). Mass spectrometry proteomics data have been deposited in the Proteome Xchange Consortium (http://proteomecentral.roteomexchange.org) via the PRIDE partner repository (Vizcaino et al., 2013) with the dataset identifier, PXD004103.

Definition of VRK1/3-interacting proteins

For analysis of comparative proteomics, proteins with more than two unique peptides and lower than 0.01 posterior error probability were selected. We additionally removed all the reverse sequences and contaminant proteins. Using LFQ intensity, which represents the quantity of each identified proteins; fold change was calculated with the equation described in a previous report (Yoon et al., 2011).

$$fold\ change = \frac{\text{LFQ samle - LFQ control}}{Max\ (LFQ\ sample,\ LFQ\ control)}$$

LFQ sample: Label-free quantitative intensity of each identified protein in the VRK1/VRK3-flag co-IP samples

LFQ control: Label-free quantitative intensity of each identified protein in the flag co-IP samples. VRK1/VRK3-interacting candidate proteins were identified as those enriched in the VRK1/VRK3-positive sets, respectively, displaying more than 0.5-fold change, which means at least 50% of proteins identified more in the VRK1/VRK3-positive experimental set compared to VRK1/VRK3-negative control set.

Subcellular localization and phosphorylation of proteins

To analyze subcellular localization and phosphorylation of the proteome, we extracted the related information from UniProt. *P*-values for localization and phosphorylation of proteins compared with the whole proteome were assessed by Fisher's test. *P*-values for phosphorylated residues per protein were obtained by use of the Student's *t*-test.

Systematic analysis

DAVID 6.7 was employed for Gene Ontology analysis. Biological Process terms of Gene Ontology were used, and *P*-values were calculated with modified Fisher's exact test. The protein-protein interaction database from the NCBI Entrez Gene, updated on Feb 17 in 2013, was applied to build the hypothetical network, which was visualized with Cytoscape 2.8.3.

Cell culture, reagents and plasmids

The SK-Hep1, Hep3B, Huh-7, HepG2 and SNU449 cell lines were obtained from the Korean Cell Line Bank (Korea). SH-J1 cells were provided by Dr. Dae-Ghon Kim (Medical School, Chonbuk National University) (Kim et al., 2002). HEK293FT and THLE-2 cells were purchased from Invitrogen and American Type Culture Collection (USA), respectively. HEK293FT and liver cancer cells were cultured at 37℃ under 5% CO_2 in DMEM supplemented with 10% FBS, 100 units/ml of penicillin and 100 μg/ml streptomycin. THLE-2 cells originated from human primary normal liver cells were plated on culture plates pre-coated with a solution containing 0.01 mg/ml fibronectin, 0.03 mg/ml bovine collagen type I and

0.01 mg/ml bovine serum albumin dissolved in Bronchial Epithelium Basal Medium (BEBM, Lonza). THLE-2 cells were cultured at 37℃ under 5% CO2 in BEBM supplemented with Bronchial Epithelium Cell Growth Medium (BEGM) SingleQuots (Lonza). Lipofectamine 2000 (Invitrogen) was used to transfect expression vectors into cells. The same control, VRK1, VRK3 and p53 expression vectors were used as described previously (Kang and Kim, 2006; Kang et al., 2008; Lee et al., 2015b).

Small interfering RNAs (SiRNAs) and electrophoresis

For VRK3 gene silencing, cells were transfected with duplex siRNA specifically targeting VRK3 or negative control. siRNAs were synthesized from Bioneer (Korea) and sequences are following; negative control, 5'-CCU ACG CCA CCA AUU UCG U(dTdT)-3'; siVRK3, 5'-GGA CAA AUU GCC UUC CCA A(dTdT)-3'. Transient transfections for siRNAs were performed by electroporation using a Microporator MP-100 (Digital Bio) or Neon-Transfection System (Invitrogen).

SDS-PAGE and Western blotting

Co-immunoprecipitation samples were subjected to SDS-PAGE on acrylamide gel. For Commassie blue staining, the acrylamide gel was stained with Brilliant Blue R250 Protein solution (Elpis, Korea) for 1 h with gentle agitation and then washed three times with destaining solution containing 20% methanol and 10% acetic acid for 1 h. For Western blotting, SDS-PAGE gel was transferred onto PVDF membranes (Millipore). After blocking with 5% skimmed milk in TBS-T buffer (50 mM Tris-HCl, pH 7.4, 150 mM NaCl, 0.1% Tween20) for 1 h, membranes were incubated with the primary antibodies at 4℃ with shaking overnight. After incubated with the secondary antibody for 2 h, immunocomplexes were detected by use of the femto, Pico or ECL reagent (Thermo). Antibodies for Western blotting are from the companies as follows: mouse/rabbit anti-flag antibody (Sigma), mouse anti-VRK1 (Santa Cruz), rabbit anti-VRK3 (Sigma), mouse ant-ALY antibody (Santa Cruz), rabbit anti-hsp70 (Origene), rabbit anti-XRCC5 (Santa Cruz), rabbit anti-B23 antibody (Santa Cruz), rabbit anti-C23 antibody (Santa Cruz), rabbit anti-PARP1 antibody (Cell signaling), rabbit anti-cyclin B1 (Santa Cruz), rabbit anti-p53 (Cell signaling) and rabbit anti-BAF [previously used (Kim et al., 2015)].

Immunocytochemical staining

HEK293FT cells were seeded on cover slips coated with poly-D-lysine, fixed with 4% paraformaldehyde in PBS, permeabilized with 0.1% Triton X-100 in PBS, and subsequently blocked with 1% BSA in PBS for 1 h. To verify the cellular localization of VRK1 and VRK3 expressed ectopically, the cells were incubated with mouse/rabbit anti-GFP antibody (Sigma) in the 4℃ overnight. The cells were washed with PBS three times and incubated with anti-mouse/rabbit Alexa Fluor 488 (Invitrogen) and anti-rabbit/mouse/goat Alexa Fluor 594 (Invitrogen) for 1 h at room temperature in the dark. Cells were subsequently washed with PBS, incubated with Hoechst 33342 (Invitrogen) for 10 min at room temperature, and mounted with Mounting medium (Dako).

Detection of phosphorylated proteins

To detect phosphorylated interacting proteins, we performed immunoprecipitation experiments using mouse anti-phospho (p)-serine (Sigma) or mouse anti-phospho (p)-threonine antibodies (Santa Cruz), as previously described (Lee et al., 2015a). Briefly, transfected cells were suspended in 180 μl lysis buffer and 20 μl 10% SDS (final concentration of SDS, 1%). The samples were boiled for 10 min to denature proteins. Then, 1.8 ml of lysis buffer containing protease and phosphatase inhibitors was added to the samples (final concentration of SDS, 0.1%). The lysates were immunoprecipitated overnight 4℃ with 2 μl of anti-p-serine or anti-p-threonine antibody, and 30 μl of protein G agarose beads were added and incubated for an additional 2 h. The beads were washed three times with lysis buffer, and the precipitated proteins were eluted in Laemmli 2× sample buffer (Sigma) at 100℃ for 5 min. Phosphorylated interacting candidates were detected by immunoblotting using rabbit cyclin B1 (Cell signaling) and rabbit anti-XRCC5 (Santa Cruz) antibodies.

Gene expression data

In an attempt to compare the mRNA levels of VRK1/VRK3 in non-tumor tissues and HCC, Gene expression data was obtained from the National Center for Biotechnology Information (NCBI) Gene Expression Omnibus (GEO) database (accession numbers are GSE57958 and GSE45436).

Cell cycle analysis

To analyze the progression of the cell cycle on asynchronous cell populations, 8×10^4 cells were seeded onto 6-well plates, transiently transfected with negative control or VRK3-specific siRNA and grown for 36 h. Cells were then collected by trypsinization, fixed in the fixation solution containing 70% ethanol and 0.5% Tween-20, washed with PBS containing 1% BSA, resuspended in 200 μl PBS containing 100 μg/ml RNase (Sigma) and 50 μg/ml propidium iodide (Sigma), incubated in the dark for 40 min at room temperature, and analyzed using the Canto II flow cytometer (BD Biosciences). Acquired data were analyzed using ModFit LT software (Verity Software House). Four independent experiments were performed.

RESULTS AND DISCUSSION

Identification of VRK1- and VRK3-interacting proteins by LC-MS/MS

To identify VRK1/VRK3-interacting proteins, we performed sequential experiments as shown in Fig. 1A. Initially, the flag-conjugated VRK1/VRK3 expression vectors were transiently transfected into HEK293FT cells, which have been widely used to identify interacting proteins by co-immunoprecipitation coupled with mass spectrometry (Law et al., 2009; 2014; Miteva and Cristea, 2013; Tsai et al., 2012). Artificial tagging can mislocalize proteins within cells, therefore, we verified the localization of flag-tagged VRK1/VRK3 proteins by immunofluorescent staining. Ectopically expressed VRK1/VRK3 proteins were clearly localized in the nucleus of most cells in agreement with previous findings (Fig. 1B) (Roopra et al., 2004). Using anti-flag affinity gel, flag-tagged VRK1/VRK3

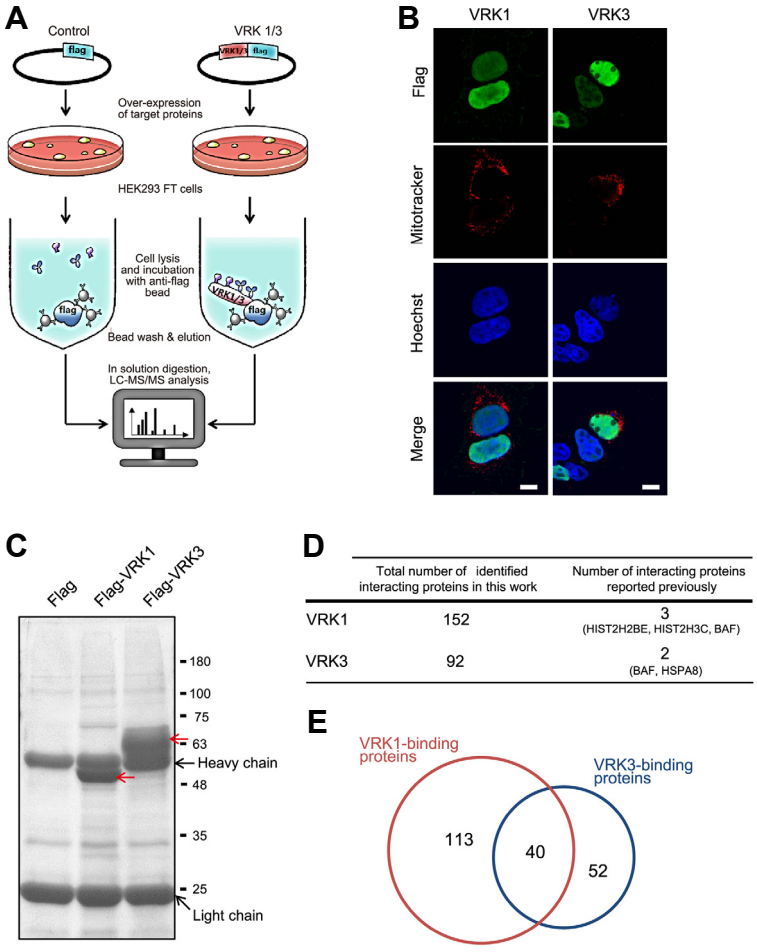

Fig.1. Experimental scheme and analysis of VRK1- and VRK3-interacting proteins. (A) Experimental procedures for affinity purification coupled with LC-MS/MS analysis. Flag-tagged VRK1 and VRK3 proteins were expressed in HEK293FT cells and immunoprecipitated with anti-flag antibody immobilized on affinity gels. Immuno-complexes were eluted and digested for LC-MS/MS analysis. (B) Localization of transiently expressed VRK1 and VRK3. HEK293FT cells transfected with VRK1-flag and VRK3-flag expressing vector were fixed after 24 h, followed by probing with flag antibody and mitotraker. Arrows indicate the cytoplasmic localization of VRK1 and VRK3. Images magnified 400X. Scale bar indicates 10 μm. (C) SDS-PAGE and Coomassie blue staining of immunocomplexes. The arrow on the second and third lanes indicates VRK1 and VRK3, respectively. (D) Comparison of interacting proteins with those reported previously for VRK1- and VRK3-interacting proteins. (E) Venn diagram comparing VRK1- and VRK3-interactomes.

proteins were isolated together with bound proteins. The enrichment of VRK1/VRK3 with interacting proteins by co-immunoprecipitation was confirmed by SDS-PAGE analysis (Fig. 1C). VRK1/VRK3 and co-isolated proteins were enriched from the affinity gel (Fig. 1C). The same samples were also used for in-solution digestion using a spin filter (Manza et al., 2005; Wisniewski et al., 2009) and LC-MS/MS analysis of tryptic peptides with an LTQ Velos Orbitrap mass spectrometer, which was performed in triplicate. A database search using MaxQuant software followed by LFQ revealed VRK1/VRK3-interacting candidate proteins. We characterized 174 and 144 proteins (Supplementary Table 1) from a total of 996 and 574 unique peptides, respectively (Supplementary Table 2), using the in-solution digested samples. We selected candidate proteins with unique peptides identified more than twice with a posterior error probability of lower than 0.01 for further analysis and eliminated all reverse sequences and contaminant proteins. We enriched 152 potential interacting candidates for VRK1 and 92 potential interacting candidates for VRK3 (Fig. 1D; Supplementary Table 3). We identified three interacting proteins of VRK1 and two interacting proteins of VRK3 that had been identified previously (Fig. 1D). Overall, the interactomes we identified for VRK1/VRK3 contained many novel VRK1- and VRK3-interacting candidate proteins. To confirm a functional link between VRK1 and VRK3, we compared their binding partners. We identified 40 common potential interacting partners (Fig. 1E), implying that VRK1 and VRK3 share common functions.

Systematic analyses of VRK1/VRK3 interactomes

We investigated the biological relevance of the VRK1/VRK3 interactomes. First, we confirmed the subcellular localizations of VRK1/VRK3-interacting candidate proteins. Nuclear and cytoplasmic proteins were enriched, reflecting the nuclear and cytoplasmic localization of VRK1/VRK3 (Fig. 2A). Because VRK1 and VRK3 are kinases, we measured the percentages of phosphorylated proteins and found that the proportion of phosphorylated proteins were significantly higher in the VRK1 and VRK3 interactomes than in the whole proteome (whole proteome, 8.7%; VRK1 interactome, 71.7%; VRK3 interactome, 77.2%; $P > 0.05$; Fig. 2B).

Network analysis of VRK1/VRK3 interactomes

Functional enrichment and subsequent interactome analyses reflected various functions of VRK1/VRK3, including chromatin assembly, RNA processing, cell cycle, and DNA repair. To confirm proteins corresponding to specific functions, we

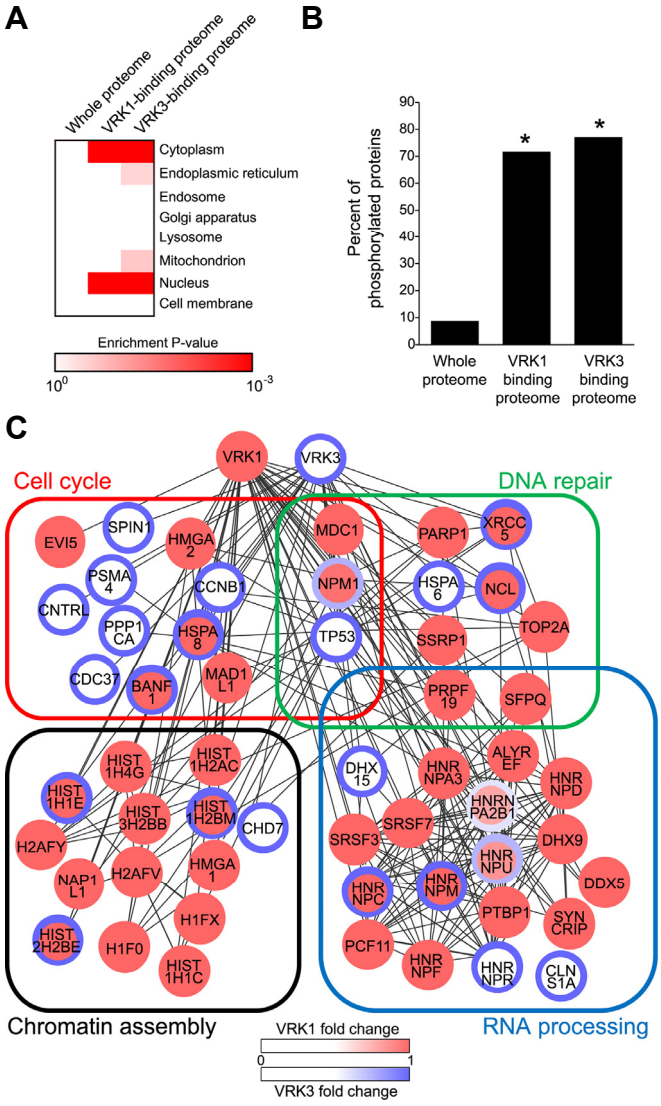

Fig. 2. Systematic Analysis of VRK1 and VRK3 interactomes. (A) Subcellular localizations of VRK1 and VRK3 interactomes. (B) Percent of phosphorylated proteins in the whole proteome and VRK1 and VRK3 interactomes. Fisher's test was used for statistical analysis. ($*P < 0.001$) (C) GO biological process network delineating the relationship between VRK1- and VRK3-interacting proteins. The intensity of node colors indicates fold change of interacting proteins in co-IP samples. Red and blue circles indicate the enrichment of indicated proteins in VRK1 and VRK3 co-IP samples, respectively. Each functional module of the interacting partners outlined with color; cell cycle (red), DNA repair (green), chromatin assembly (black) and RNA processing (blue). Edges were drawn based on the public protein-protein interaction database (gray).

established a network model utilizing the VRK1- and VRK3-interacting candidate proteins involved in these four functions (chromatin assembly, RNA processing, cell cycle, and DNA repair; Fig. 2C). In the network analysis, 12 common potential interacting proteins, 29 VRK1-interacting candidate proteins, and 11 VRK3-interacting candidate proteins were identified. Consistent with previous findings (Gorjanacz et al., 2007; Park et al., 2015), BAF was identified in both VRK1 and VRK3 interactomes (Fig. 2C). This interaction is crucial for VRK1 and VRK3 function in cell cycle progression. VRK1 phosphorylates BAF at three sites, Ser4 and/or Thr2/Thr3, for the progression of mitosis (Nichols et al., 2006). VRK3 phosphorylates BAF at Ser4 for DNA replication during interphase (Park et al., 2015). We also identified 10 novel VRK1- or VRK3-interacting candidate proteins involved in the cell cycle, including cyclin B1 (CCNB1), centriolin (CTNRN), and spindlin-1 (SPIN1) (Fig. 2C). Interestingly, SPIN1, a meiotic spindle-binding protein, was suggested to be phosphorylated in a cell cycle-dependent manner and plays a role in cell cycle regulation (Oh et al., 1997). Although SPIN1 phosphorylation on Thr 95 was reported to be crucial for its proper functions (Zhao et al., 2007), a kinase phosphorylating SPIN1 has not been identified yet. Because SPIN1 was identified as a VRK3-interacting candidate proteins, it may be phosphorylated by VRK3. CTNRN is a centrosome component that regulates cell cycle progression during interphase and mitosis (Hinchcliffe, 2003). Regulators for CTNRN have not been identified. Because CTNRN and SPIN1 are critical for cell cycle progression, VRK3-mediated regulation of SPIN1 or CTNRN functions in cell cycle should be investigated further.

Our interactomes included 10 novel VRK1/VRK3-interacting candidate proteins involved in DNA repair, such as nucleophosmin (NPM1), nucleolin (NCL), X-ray repair cross-complementing protein 5 (XRCC5), heat shock 70 kDa protein 1A/1B (HSPA1A), and poly [ADP-ribose] polymerase 1 (PARP1) (Fig. 2C). Phosphorylation of these proteins is important for their functions. For example, phosphorylation is crucial for maximal PARP1 activation after DNA damage

(Kauppinen et al., 2006). Phosphorylated NPM1 is recruited to the foci of DNA damage and promotes Ring Finger Protein 8-dependent DNA repair (Koike et al., 2010). Because those proteins have been identified as VRK1/ VRK3-interacting candidate proteins, VRK1/ VRK3 might regulate the phosphorylation of these proteins.

Proteins involved in RNA processing such as heterogeneous nuclear ribonucleoproteins (hnRNPs) and THO complex subunit 4 (ALYREF) were also identified in our interactomes (Fig. 2C). ALYREF and HnRNPs are RNA-binding proteins and are involved in RNA processing (Han et al., 2010). We previously reported the interaction of HnRNP A1 with VRK1 (Choi et al., 2012), but the association of VRK1 or VRK3 with RNA processing needs to be investigated. Many histones involved in chromatin assembly were also identified as VRK1- and VRK3-interacting candidate proteins (Fig. 2C). Nuclear VRK1 and VRK3 might regulate chromatin structure and gene expression by phosphorylating histone proteins. Thus, the interactomes we have identified for VRK1 and VRK3 imply crucial roles in the cell cycle, DNA repair, RNA processing, and chromatin assembly.

Confirmation of the specific interactions between VRK1/VRK3 and their binding proteins

We demonstrated that VRK1 and VRK3 interact with proteins involved in DNA repair, the cell cycle, and RNA processing by co-immunoprecipitation and Western blotting. These interaction partners included NCL, PARP1, HSP70, XRCC5, TP53, NPM1, BAF, CCNB1, and ALYREF. We co-immunoprecipitated these proteins with VRK1/VRK3 in VRK1/3-expressing HEK293FT cell lysates, except for TP53 and CCNB1, which were only detected in VRK3-enriched samples consistent with our mass spectrometry data (Figs. 3A and 3B). Interestingly, TP53 was not co-immunoprecipitated with VRK1 in detectable quantities under our experimental conditions. TP53 was previously shown to be a VRK1 substrate (Lopez-Borges and Lazo, 2000; Lopez-Sanchez et al., 2014; Vega et al., 2004); therefore, we further tested the interaction of VRK1 and VRK3 with p53 by reciprocal co-immunoprecipitation. Consistent with our mass spectrometry data, only VRK3, not VRK1, was co-immunoprecipitated with p53 (Supplementary Fig. 1A). This discrepancy with previous reports might be explained by different conditions of immunoprecipitation. Because VRK3 strongly binds with p53, p53 might be a direct substrate of VRK3. Specific binding of VRK3 to CCNB1 implies that VRK1 and VRK3 are functionally linked by shared interaction proteins and execute distinct functions by regulating specific target proteins.

Phosphorylation levels of XRCC5 and cyclin B1 by VRK1/VRK3

As VRK1 and VRK3 are kinases, we investigated the phos-

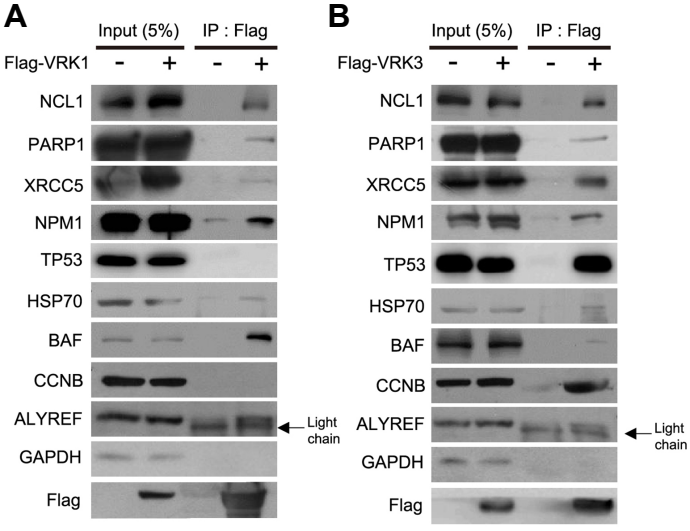

Fig. 3. Validation of interacting proteins with VRK1 and VRK3. Co-immunoprecipitation of interacting proteins with VRK1 (A) and VRK3 (B). Co-immunoprecipitation was performed by mixing flag antibody-conjugated beads with cell lysates of HEK293FT cells transfected transiently with pCMV_flag, pCMV_VRK1-flag and pCMV_VRK3-flag. Target proteins associated with cell cycle or DNA repair such as NCL, PARP1, HSP70, XRCC5, p53, NPM1, BAF and CCNB, and RNA processing such as ALYREF were confirmed by Western blotting.

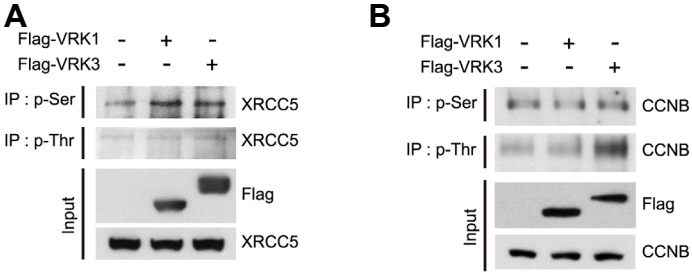

Fig. 4. Phosphorylation levels of XRCC5 and CCNB by expression of VRK1 or VRK3. Phosphorylation levels of XRCC5 (A) and CCNB (B) upon the overexpression of VRK1 or VRK3. Expression vectors for flag, VRK1-flag and VRK3-flag, were transfected into HEK293FT cells. After 24 h, cells were lysed, immunoprecipitated with anti-phosphoserin or anti-phosphothreonine antibodies immobilized on agarose beads, and then subjected to Western blotting.

phorylation of interaction partners. We first checked the phosphorylation levels of XRCC5 which could bind to both VRK1 and VRK3 (Fig. 4A). We overexpressed VRK1/VRK3 in HEK293FT cells using expression vectors. Immunoprecipitation using anti-phosphoserine or anti-phosphothreonine antibodies enriched phosphorylated proteins, and changes in the phosphorylation levels of interacting proteins were confirmed by Western blotting of interacting proteins. Phosphorylated serine residues on XRCC5 were increased by VRK1 or VRK3 overexpression, suggesting that both VRK1 and VRK3 might regulate phosphorylation levels of XRCC5. Though phosphorylation sites of XRCC5 have been identified (Douglas et al., 2005), the role of phosphorylation on XRCC5 is unclear. Thus, roles of VRK1/VRK3-mediated phosphorylation on XRCC5 are warrant for further investigation.

We next confirmed the phosphorylation levels of cyclin B1 which specifically binds to VRK3. The phosphorylation levels of cyclin B1 at threonine residues were increased after VRK3 overexpression (Fig. 4B), indicating that cyclin B1 is phosphorylated by VRK3. VRK1 overexpression did not affect the phosphorylation levels of cyclin B1 (Fig. 4B), indicating specific regulation of cyclinB1 by VRK3. Phosphorylation of cyclin B1 at serine residues is important for its nuclear translocation (Li et al., 1997). Polo-like kinase (Plk)-1 is a cyclin B1 kinase that phosphorylates Ser147 and/or Ser133 (Toyoshima-Morimoto et al., 2001). Interestingly, we found that VRK3 may also be a kinase for cyclin B1. Unlike Plk1, VRK3 phosphorylated cyclin B1 at threonine residues. Elucidation of the specific cyclin B1 threonine residues that are phosphorylated by VRK3 and the physiological relevance of this phosphorylation should contribute to our understanding of the molecular role of VRK3 during cell cycle progression.

Distinct effect of VRK3 on the cell cycle progression of liver cancer

Since VRK1 and VRK3 specifically bind to distinct interacting proteins involved in cell cycle such as EVI5, HMGA2, MAD1L1 for VRK1 and CCNB, SPIN1, CNTRL etc. for VRK3 (Fig. 2C), respectively, we tested whether VRK3 could differently affect the cell cycle progression compared with VRK1. We previously reported that VRK1 could promote liver cancer progression by promoting G1/S transition (Lee et al., 2015b). Thus we chose the liver cancer as an experimental model system to compare the effects of VRK3 and VRK1 on the cell cycle progression of liver cancer. We first checked the expression levels of VRK3 in the liver cancer. VRK3 levels were higher in six liver cancer cell lines than THLE-2 cell line, an immortalized cell line (Fig. 5A). Consistently, publicly available datasets showed high expressions of VRK3 in hepatocellular carcinoma (HCC) tissues compared with non-tumor

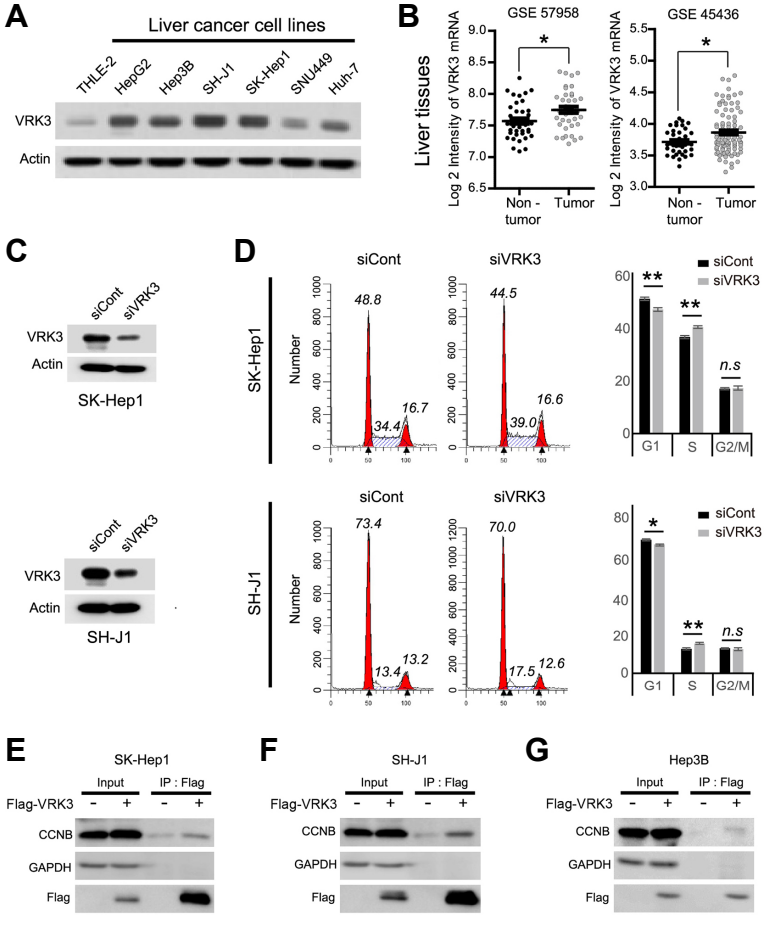

Fig. 5. Characterization of interaction of CCNB with VRK3 in the liver cancer. (A) The levels of VRK3 in THLE-2 cells immortalized normal cell line, and six liver cancer cell lines were analyzed by Western blotting. (B) Analysis of VRK3 expression in HCC and non-tumor tissues using microarray dataset obtained from the GEO database. Student's t-test was used for statistical analysis. ($*P < 0.05$) (C) Expression levels of VRK3 in SK-Hep1 and SH-J1. VRK3 levels were reduced in the SK-Hep1 and SH-J1 cells 36 h after transfection with VRK3 siRNA as judged by Western blotting. (D) Cell cycle analysis of VRK3-depleted SK-Hep1 and SH-J1. SK-Hep1 and SH-J1 were transfected with control and VRK3 siRNAs and grown for 36 h, after which they were stained with propidium iodide (PI) and subjected to FACS analysis. The number of SK-Hep1 and SH-J1 cells at G1, S and G2/M phase was quantified. The Modifit program was used for data analysis. Four independent experiments were performed and representative FACS data are shown (left). The percentages of cells at G1, S and G2/M phase are indicated in the histogram (right). (n.s., not significant; $*P < 0.05$; $**P < 0.01$) (E-G) Co-immunoprecipitation of CCNB with VRK1 in SK-Hep1 (E), SH-J1 (F) and Hep3B (G). Co-immunoprecipitation was performed by mixing flag antibody-conjugated beads with cell lysates of three liver cancer cell lines transfected transiently with pCMV_flag or pCMV_VRK3-flag, and then subjected to Western blotting.

tissues (Fig. 5B). We also confirmed high expression of VRK1 in HCC tissues and liver cancer cell lines using the same datasets as well as in the same liver cancer cell lines (Supplementary Fig. 2A), which is consistent with our previous report showing oncogenic potential of VRK1 in liver cancer (Lee et al., 2015b).

To understand the effect of VRK3 on cell cycle of liver cancer cells, we performed FACS analyses after transfection with control or VRK3 siRNA. Western blotting showed that VRK3 was efficiently silenced by transfection of VRK3 siRNA in SK-Hep1 and SH-J1 cells (Fig. 5C). Interestingly, the number of S phase gated cells was significantly higher in VRK3 depleted-SK-Hep1 and SH-J1 cells than control cells, whereas the number of G1 phase gated cells was lower in VRK3 depleted cells than control cells (Fig. 5D). The number of G2/M phase gated cells were not changed by VRK3 silencing (Fig. 5D). These data indicate distinct effects of VRK3 in cell cycle progression of liver cancer cell when compared with VRK1 whose depletion induced the G1 arrest (Lee et al., 2015b). We think that different effects of VRK1 and VRK3 on cell cycle progression could be mediated by different interacting proteins. Thus, we re-validated the interaction of CCNB1 with VRK3 in three liver cancer cell lines, because CCNB1 was identified to specifically bind to VRK3 in HEK293FT cells. In addition, CCNB1 has been shown to regulate not only mitosis entry (Gavet and Pines, 2010) and exit (Potapova et al., 2006), but also S phase progression (Moore et al., 2003). Consistent with our result, CCNB1 was clearly co-immunoprecipitated with VRK3 in three liver cancer cell lines (Figs. 5E-5G).

Figure 6 shows the schematic model of the distinct roles of VRK1 and VRK3 in the cell cycle progression of liver cancer. Our group previously reported that VRK1 regulates the G1/S transition via phosphorylating the CREB protein which upregulates CCND1, thus VRK1 depletion induces the G1 arrest (Lee et al., 2015b). Interestingly, in this study, we found that VRK3 could also affect cell cycle progression but it seemed to regulate different stage of cell cycle progression in liver cancer. A higher number of S phase gated cells in VRK3 silenced cells might indicate that VRK3 depletion induced S phase arrest. If VRK3-depleted cells have defects only in S phase, the number of both G1 and G2/M phase gated cells should be decreased in VRK3 depleted cells than control cells in the cell cycle. However, the number of G2/M phase gated cells was not changed by VRK3 depletion, even though G1 phase gated cells were decreased in VRK3 depleted cells (Fig. 5D). Thus, VRK3-depleted cells might also have defects in G2 or M phase entry and exit. These phenomena could be related with the roles of VRK3-interacting candidate proteins. First, CCNB1 is crucial for the progression of the cells entry (Gavet and Pines, 2010) and exit (Potapova et al., 2006) of M phase. CCNB1 also has S-phase promoting abilities (Moore et al., 2003). Thus, VRK3 defects might affect the activity of CCNB1 via regulation of phosphorylation levels, which results in the defects on M phase entry and exit and/or S phase progression. Second, CTNRL is necessary for a late stage of cytokinesis, the cytoplasmic division of a cell at the end of mitosis (Hinchcliffe, 2003). CTNRL is involved in the spindle position checkpoint. CTNRL deficiency induces improper spindle position, which results in M phase arrest (Pereira and Schiebel, 2001). Thus, the effect of VRK3 on G2/M phase might be mediated by CTNRL functions. Third, overexpression of SPIN1 was known to have a different cell cycle distribution in S and G2/M phases (Gao et al., 2005; Zhao et al., 2007). Phosphorylation levels of SPIN1 are also altered in the cell cycle-dependent fashion (Oh et al., 1997). Thus, the effect of VRK3 on G2/M or S phase might be mediated by functions of SPIN1. Though we explained the defects of cell cycle progression by VRK3 silencing via known functions of interacting candidates, our model remains to be investigated to elucidate the molecular role of VRK3 during the cell cycle progression.

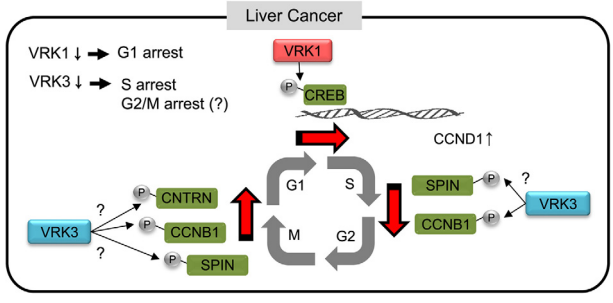

Fig. 6. Schematic diagram of the distinct roles of VRK1 and VRK3 during the cell cycle progression in liver cancer.

CONCLUSION

We systematically identified the proteins that interact with VRK1/VRK3 by affinity purification coupled with LC-MS/MS analysis. Using this approach, we identified novel VRK1/VRK3-interacting candidate proteins while confirming those which were already known. We validated interactions of the novel candidate proteins with VRK1/VRK3 by co-immunoprecipitation. VRK1/VRK3 regulated the phosphorylation of XRCC5. The phosphorylation of CCNB was specifically regulated by VRK3. We also suggested distinct effects of VRK1 and VRK3 on cell cycle progression in liver cancer, which could be affected differentially by distinctly different interacting candidate proteins. VRK3 seemed to affect S phase progression and G2 or M phase entry and exit, whereas VRK1 affects G1/S transition in the liver cancer. Overall, this study provides a resource for studying VRK1 and VRK3 functions as well as evidences that VRK1/VRK3 are functionally important in cell cycle regulation, mRNA processing, chromatin assembly, and DNA repair.

Note: Supplementary information is available on the Molecules and Cells website (www.molcells.org).

ACKNOWLEDGMENTS

This study was supported by a grant from the Next-Generation BioGreen 21 Program, Rural Development Administration, Republic of Korea (Project No. PJ01121601) and KBRI basic research program through Korea Brain Research Institute funded by the Ministry of Science, ICT and

Future Planning (Project No. 17-BR-01). D.-K. Kim was supported by a National Junior Research Fellowship funded by Ministry of Education, Science and Technology, Republic of Korea. H.G.R. is supported by a KT&G Scholarship Foundation (KT&G, Korea). We thank Ohseop Kwon for designing the image for the experimental scheme in our manuscript.

REFERENCES

Choi, D.S., Kim, D.K., Choi, S.J., Lee, J., Choi, J.P., Rho, S., Park, S.H., Kim, Y.K., Hwang, D., and Gho, Y.S. (2011). Proteomic analysis of outer membrane vesicles derived from Pseudomonas aeruginosa. Proteomics *11*, 3424-3429.

Choi, Y.H., Lim, J.K., Jeong, M.W., and Kim, K.T. (2012). HnRNP A1 phosphorylated by VRK1 stimulates telomerase and its binding to telomeric DNA sequence. Nucleic Acids Res. *40*, 8499-8518.

Douglas, P., Gupta, S., Morrice, N., Meek, K., and Lees-Miller, S.P. (2005). DNA-PK-dependent phosphorylation of Ku70/80 is not required for non-homologous end joining. DNA Repair *4*, 1006-1018.

Gao, Y., Yue, W., Zhang, P., Li, L., Xie, X., Yuan, H., Chen, L., Liu, D., Yan, F., and Pei, X. (2005). Spindlin1, a novel nuclear protein with a role in the transformation of NIH3T3 cells. Biochem. Biophys. Res. Commun. *335*, 343-350.

Gavet, O., and Pines, J. (2010). Progressive activation of CyclinB1-Cdk1 coordinates entry to mitosis. Dev. Cell *18*, 533-543.

Gorjanacz, M., Klerkx, E.P., Galy, V., Santarella, R., Lopez-Iglesias, C., Askjaer, P., and Mattaj, I.W. (2007). Caenorhabditis elegans BAF-1 and its kinase VRK-1 participate directly in post-mitotic nuclear envelope assembly. EMBO J. 26, 132-143.

Han, S.P., Tang, Y.H., and Smith, R. (2010). Functional diversity of the hnRNPs: past, present and perspectives. Biochem. J.430, 379-392.

Hinchcliffe, E.H. (2003). Cell cycle: seeking permission from the mother centriole. Curr. Biol. 13, R646-648.

Joshi, P., Greco, T.M., Guise, A.J., Luo, Y., Yu, F., Nesvizhskii, A.I., and Cristea, I.M. (2013). The functional interactome landscape of the human histone deacetylase family. Mol. Syst. Biol. *9*, 672.

Kang, T.H., and Kim, K.T. (2006). Negative regulation of ERK activity by VRK3-mediated activation of VHR phosphatase. Nat. Cell Biol. *8*, 863-869.

Kang, T.H., Park, D.Y., Choi, Y.H., Kim, K.J., Yoon, H.S., and Kim, K.T. (2007). Mitotic histone H3 phosphorylation by vaccinia-related kinase 1 in mammalian cells. Mol. Cell. Biol. *27*, 8533-8546.

Kang, T.H., Park, D.Y., Kim, W., and Kim, K.T. (2008). VRK1 phosphorylates CREB and mediates CCND1 expression. J. Cell Sci. *121*, 3035-3041.

Kauppinen, T.M., Chan, W.Y., Suh, S.W., Wiggins, A.K., Huang, E.J., and Swanson, R.A. (2006). Direct phosphorylation and regulation of poly(ADP-ribose). polymerase-1 by extracellular signal-regulated kinases 1/2. Proc. Natl. Acad. Sci. USA *103*, 7136-7141.

Kim, D.G., Park, S.Y., Kim, H., Chun, Y.H., Moon, W.S., and Park, S.H. (2002). A comprehensive karyotypic analysis on a newly established sarcomatoid hepatocellular carcinoma cell line SH-J1 by comparative genomic hybridization and chromosome painting. Cancer Genet. Cytogenet. *132*, 120-124.

Kim, W., Chakraborty, G., Kim, S., Shin, J., Park, C.H., Jeong, M.W., Bharatham, N., Yoon, H.S., and Kim, K.T. (2012). Macro histone H2A1.2 (macroH2A1). protein suppresses mitotic kinase VRK1 during interphase. J. Biol. Chem. *287*, 5278-5289.

Kim, S.H., Lyu, H.N., Kim, Y.S., Jeon, Y.H., Kim, W., Kim, S., Lim, J.K., Lee, H.W., Baek, N.I., Choi, K.Y., et al. (2015). Brazilin Isolated from Caesalpinia sappan suppresses nuclear envelope reassembly by inhibiting barrier-to-autointegration factor phosphorylation. J. Pharmacol. Exp. Ther. *352*, 175-184.

Klerkx, E.P., Lazo, P.A., and Askjaer, P. (2009). Emerging biological functions of the vaccinia-related kinase (VRK). family. Histol. Histopathol. *24*, 749-759.

Koike, A., Nishikawa, H., Wu, W., Okada, Y., Venkitaraman, A.R., and Ohta, T. (2010). Recruitment of phosphorylated NPM1 to sites of DNA damage through RNF8-dependent ubiquitin conjugates. Cancer Res. *70*, 6746-6756.

Law, I.K., Liu, L., Xu, A., Lam, K.S., Vanhoutte, P.M., Che, C.M., Leung, P.T., and Wang, Y. (2009). Identification and characterization of proteins interacting with SIRT1 and SIRT3: implications in the anti-aging and metabolic effects of sirtuins. Proteomics *9*, 2444-2456.

Lee, N., Kim, D.K., Kim, E.S., Park, S.J., Kwon, J.H., Shin, J., Park, S.M., Moon, Y.H., Wang, H.J., Gho, Y.S., et al. (2014). Comparative interactomes of SIRT6 and SIRT7: Implication of functional links to aging. Proteomics *14*, 1610-1622.

Lee, M.S., Jeong, M.H., Lee, H.W., Han, H.J., Ko, A., Hewitt, S.M., Kim, J.H., Chun, K.H., Chung, J.Y., Lee, C., et al. (2015a). PI3K/AKT activation induces PTEN ubiquitination and destabilization accelerating tumourigenesis. Nat. Commun. *6*, 7769.

Lee, N., Kwon, J.H., Kim, Y.B., Kim, S.H., Park, S.J., Xu, W., Jung, H.Y., Kim, K.T., Wang, H.J., and Choi, K.Y. (2015b). Vaccinia-related kinase 1 promotes hepatocellular carcinoma by controlling the levels of cell cycle regulators associated with G1/S transition. Oncotarget *6*, 30130-30148.

Li, J., Meyer, A.N., and Donoghue, D.J. (1997). Nuclear localization of cyclin B1 mediates its biological activity and is regulated by phosphorylation. Proc. Natl. Acad. Sci. USA *94*, 502-507.

Lopez-Borges, S., and Lazo, P.A. (2000). The human vaccinia-related kinase 1 (VRK1). phosphorylates threonine-18 within the mdm-2 binding site of the p53 tumour suppressor protein. Oncogene *19*, 3656-3664.

Lopez-Sanchez, I., Sanz-Garcia, M., and Lazo, P.A. (2009). Plk3 interacts with and specifically phosphorylates VRK1 in Ser342, a downstream target in a pathway that induces Golgi fragmentation. Mol. Cell. Biol. *29*, 1189-1201.

Lopez-Sanchez, I., Valbuena, A., Vazquez-Cedeira, M., Khadake, J., Sanz-Garcia, M., Carrillo-Jimenez, A., and Lazo, P.A. (2014). VRK1 interacts with p53 forming a basal complex that is activated by UV-induced DNA damage. FEBS Lett. *588*, 692-700.

Luber, C.A., Cox, J., Lauterbach, H., Fancke, B., Selbach, M., Tschopp, J., Akira, S., Wiegand, M., Hochrein, H., O'Keeffe, M., et al. (2010). Quantitative proteomics reveals subset-specific viral recognition in dendritic cells. Immunity *32*, 279-289.

Manza, L.L., Stamer, S.L., Ham, A.J., Codreanu, S.G., and Liebler, D.C. (2005). Sample preparation and digestion for proteomic analyses using spin filters. Proteomics *5*, 1742-1745.

Miteva, Y.V., and Cristea, I.M. (2013). A proteomic perspective of Sirtuin 6 (SIRT6) phosphorylation and interactions and their dependence on its catalytic activity. Mol. Cell. Proteomics *13*, 168-183.

Monsalve, D.M., Campillo-Marcos, I., Salzano, M., Sanz-Garcia, M., Cantarero, L., and Lazo, P.A. (2016). VRK1 phosphorylates and protects NBS1 from ubiquitination and proteasomal degradation in response to DNA damage. Biochim. Biophys. Acta *1863*, 760-769.

Moore, J.D., Kirk, J.A., and Hunt, T. (2003). Unmasking the S-phase-promoting potential of cyclin B1. Science *300*, 987-990.

Nichols, R.J., and Traktman, P. (2004). Characterization of three paralogous members of the Mammalian vaccinia related kinase family. J. Biol. Chem. *279*, 7934-7946.

Nichols, R.J., Wiebe, M.S., and Traktman, P. (2006). The vaccinia-related kinases phosphorylate the N' terminus of BAF, regulating its interaction with DNA and its retention in the nucleus. Mol. Biol. Cell *17*, 2451-2464.

Oh, B., Hwang, S.Y., Solter, D., and Knowles, B.B. (1997). Spindlin, a major maternal transcript expressed in the mouse during the transition from oocyte to embryo. Development *124*, 493-503.

Park, C.H., Ryu, H.G., Kim, S.H., Lee, D., Song, H., and Kim, K.T. (2015). Presumed pseudokinase VRK3 functions as a BAF kinase. Biochim. Biophys. Acta *1853*, 1738-1748.

Pereira, G., and Schiebel, E. (2001). The role of the yeast spindle pole body and the mammalian centrosome in regulating late mitotic events. Curr. Opin. Cell Biol. *13*, 762-769.

Potapova, T.A., Daum, J.R., Pittman, B.D., Hudson, J.R., Jones, T.N., Satinover, D.L., Stukenberg, P.T., and Gorbsky, G.J. (2006). The reversibility of mitotic exit in vertebrate cells. Nature *440*, 954-958.

Roopra, A., Qazi, R., Schoenike, B., Daley, T.J., and Morrison, J.F. (2004). Localized domains of G9a-mediated histone methylation are required for silencing of neuronal genes. Mol. Cell *14*, 727-738.

Salzano, M., Sanz-Garcia, M., Monsalve, D.M., Moura, D.S., and Lazo, P.A. (2015). VRK1 chromatin kinase phosphorylates H2AX and is required for foci formation induced by DNA damage. Epigenetics *10*, 373-383.

Sevilla, A., Santos, C.R., Barcia, R., Vega, F.M., and Lazo, P.A. (2004a). c-Jun phosphorylation by the human vaccinia-related kinase 1 (VRK1)., and its cooperation with the N-terminal kinase of c-Jun (JNK). Oncogene *23*, 8950-8958.

Sevilla, A., Santos, C.R., Vega, F.M., and Lazo, P.A. (2004b). Human vaccinia-related kinase 1 (VRK1) activates the ATF2 transcriptional activity by novel phosphorylation on Thr-73 and Ser-62 and cooperates with JNK. J. Biol. Chem. *279*, 27458-27465.

Song, H., Kim, W., Choi, J.H., Kim, S.H., Lee, D., Park, C.H., Kim, S., Kim, D.Y., and Kim, K.T. (2016a). Stress-induced nuclear translocation of CDK5 suppresses neuronal death by downregulating ERK activation via VRK3 phosphorylation. Sci. Rep. *6*, 28634.

Song, H., Kim, W., Kim, S.H., and Kim, K.T. (2016b). VRK3-mediated nuclear localization of HSP70 prevents glutamate excitotoxicity-induced apoptosis and Abeta accumulation via enhancement of ERK phosphatase VHR activity. Sci. Rep. *6*, 38452.

Toyoshima-Morimoto, F., Taniguchi, E., Shinya, N., Iwamatsu, A., and Nishida, E. (2001). Polo-like kinase 1 phosphorylates cyclin B1 and targets it to the nucleus during prophase. Nature *410*, 215-220.

Tsai, Y.C., Greco, T.M., Boonmee, A., Miteva, Y., and Cristea, I.M. (2012). Functional proteomics establishes the interaction of SIRT7 with chromatin remodeling complexes and expands its role in regulation of RNA polymerase I transcription. Mol. Cell. Proteomics *11*, M111 015156.

Valbuena, A., Sanz-Garcia, M., Lopez-Sanchez, I., Vega, F.M., and Lazo, P.A. (2011). Roles of VRK1 as a new player in the control of biological processes required for cell division. Cell. Signal. 23, 1267-1272.

Vega, F.M., Sevilla, A., and Lazo, P.A. (2004). p53 Stabilization and accumulation induced by human vaccinia-related kinase 1. Mol. Cell. Biol. *24*, 10366-10380.

Vizcaino, J.A., Cote, R.G., Csordas, A., Dianes, J.A., Fabregat, A., Foster, J.M., Griss, J., Alpi, E., Birim, M., Contell, J., et al. (2013). The PRoteomics IDEntifications (PRIDE). database and associated tools: status in 2013. Nucleic Acids Res. *41*, D1063-1069.

Wisniewski, J.R., Zougman, A., Nagaraj, N., and Mann, M. (2009). Universal sample preparation method for proteome analysis. Nat. Methods *6*, 359-362.

Yoon, J.H., Song, P., Jang, J.H., Kim, D.K., Choi, S., Kim, J., Ghim, J., Kim, D., Park, S., Lee, H., et al. (2011). Proteomic analysis of tumor necrosis factor-alpha (TNF-alpha).-induced L6 myotube secretome reveals novel TNF-alpha-dependent myokines in diabetic skeletal muscle. J. Proteome Res. *10*, 5315-5325.

Zhao, Q., Qin, L., Jiang, F., Wu, B., Yue, W., Xu, F., Rong, Z., Yuan, H., Xie, X., Gao, Y., et al. (2007). Structure of human spindlin1. Tandem tudor-like domains for cell cycle regulation. J. Biol. Chem. *282*, 647-656.